nature communications

Article

https://doi.org/10.1038/s41467-024-47090-1

Orphan high field superconductivity in non-superconducting uranium ditelluride

Received: 28 November 2023

Accepted: 15 March 2024

Published online: 20 April 2024

Check for updates

Corey E. Frank[1,2] ✉, Sylvia K. Lewin[1,2], Gicela Saucedo Salas[1,2], Peter Czajka[1,2], Ian M. Hayes[2], Hyeok Yoon[2], Tristin Metz[2], Johnpierre Paglione[2,3], John Singleton[4] & Nicholas P. Butch[1,2] ✉

Reentrant superconductivity is an uncommon phenomenon in which the destructive effects of magnetic field on superconductivity are mitigated, allowing a zero-resistance state to survive under conditions that would otherwise destroy it. Typically, the reentrant superconducting region derives from a zero-field parent superconducting phase. Here, we show that in UTe_2 crystals extreme applied magnetic fields give rise to an unprecedented high-field superconductor that lacks a zero-field antecedent. This high-field orphan superconductivity exists at angles offset between 29° and 42° from the crystallographic *b* to *c* axes with applied fields between 37 T and 52 T. The stability of field-induced orphan superconductivity presented in this work defies both empirical precedent and theoretical explanation and demonstrates that high-field superconductivity can exist in an otherwise non-superconducting material.

Applied magnetic fields destabilize and eventually destroy superconductivity by breaking up the constituent paired electrons. In most cases, this occurs through the effect of orbital pair-breaking, a condition wherein magnetic flux cores overlap. A competing pair-breaking effect occurs at the Pauli limit, the typically higher magnetic field at which Zeeman splitting destabilizes spin anti-aligned Cooper pairs[1]. In uranium ditelluride (UTe_2) crystals that exhibit a low-field superconducting transition, however, superconductivity survives to fields that well exceed the Pauli limit, due to the occurrence of unconventional spin-triplet superconductivity[2,3]. When the magnetic field is applied along the crystallographic *b* axis, superconductivity survives to a remarkably large magnetic field value of 35 T, limited only by a first-order metamagnetic transition–a discontinuity in the magnetization– at H_m. However, if the magnetic field is tilted between a range of angles 20°–40° from the crystallographic *b*-axis towards the *c*-axis[4,5], superconductivity returns for fields greater than 40 T, persisting to approximately 70 T. The focus of this work is the relationship between this very high-field reentrant superconductivity (SC_{FP}) and the low-field phases (SC_1 and SC_2); SC_1 is generally assumed to be the primary, or "parent," superconducting phase.

The properties of the lower-field superconductivities in UTe_2 have been extensively studied, but the symmetries of the superconducting order parameter(s) have yet to be unambiguously determined[6–8]. From specific heat capacity and optical Kerr effect measurements, it was inferred that superconductivity in the lowest-field phase, SC_1, can be described by a chiral, time-reversal symmetry breaking, multi-component order parameter[6]. More recent investigations call into question the existence of a two-component order parameter and whether the state intrinsically breaks time reversal symmetry[9–11]. Evidence for a low-field point node gap structure is robust[12–14], but has recently been questioned[15]. Experimental evidence suggests that applied fields oriented along the *b* axis induce transitions between multiple superconducting phases[16], though the pairing states of and sample-dependent boundaries between these phases remain unclear[17,18].

The dominant feature in the high-field UTe_2 phase diagram when the field is nearly parallel to the *b* axis is the metamagnetic transition from either SC_2 into a field-polarized normal state at applied field H_m. The curving H_m. boundary line has a minimum of about 35 T when the field is perfectly oriented along *b* and increases smoothly as the field is

[1]NIST Center for Neutron Research, National Institute of Standards and Technology, Gaithersburg, MD, USA. [2]Maryland Quantum Materials Center, Department of Physics, University of Maryland, College Park, MD, USA. [3]Canadian Institute for Advanced Research, Toronto, ON M5G 1Z8, Canada. [4]National High Magnetic Field Laboratory, Los Alamos National Laboratory, Los Alamos, NM, USA. ✉e-mail: cef2@umd.edu; nbutch@umd.edu

rotated towards one of the other crystallographic axes. The most extraordinary aspect of this phase diagram is SC_{FP}, a pocket of zero resistance emerging at field orientations 20°–40° between *b* and *c*. The lower boundary of SC_{FP} follows H_m, which at these angles occurs at approximately 40 T[4,5].

Due to the unprecedentedly high fields required to stabilize the SC_{FP} superconducting phase, determining its pairing symmetry presents an even greater challenge than those of SC_1 and SC_2, and explorations have been limited despite plain fundamental interest[3,19–25]. It is difficult to concretely establish the nature of the relationship between the lower field superconducting phases and SC_{FP} as there are few relevant precedents. While other uranium-containing superconductors, such as URhGe[26] and UCoGe[1], exhibit field stabilized reentrant superconductivity at specific angles, these phases occur in proximity to ferromagnetic quantum critical points, whereas UTe_2 does not magnetically order below 1.4 GPa[22]. Other proposed explanations for the intense field enhancement of SC_{FP} include lowered dimensionality[20,21], which can suppress the orbital limiting effects of magnetic fields, or internal exchange fields that counteract the applied external field[3,5,27,28], leading the conduction electrons to experience smaller total magnetic fields than those applied. The commonality between these hypotheses is the assumption that high-field superconductivity represents an extension of a lower-field superconducting phase. The debate regarding SC_{FP} thus centers upon which established mechanism fortifies low field superconductivity against the deleterious effects of extreme magnetic fields. The assumptions upon which these models are based are incompatible with a superconducting phase which emerges only at extremely high-fields, and such an observation would therefore require a new form of high-field superconductivity to explain.

In this work, we present the first evidence of "orphaned" high-field superconductivity (oSC_{FP}) without an accompanying low-field "parent" phase. This unusual configuration has been achieved in UTe_2 through the controlled introduction of disorder, which destabilizes SC_1 and SC_2, while SC_{FP} unexpectedly survives at high-fields. In addition to presenting the first example of exclusively high-field-stabilized superconductivity in a uranium-based system, these findings dramatically limit possible explanations for the stability of high-field superconductivity in UTe_2 and its relation to lower field superconductivity, demanding a new theoretical framework.

Results and discussion

In the Orphan UTe_2 samples studied here, there is no evidence of SC_1 or SC_2 in any field orientation in the *bc* plane when the applied field is smaller than 35 T. Instead, the samples are paramagnetic metals which, like their low-field superconducting cousins, show evidence of Kondo lattice effects upon cooling from room temperature. Zero-field resistance measurements demonstrate Fermi-liquid T^2 dependence below 10 K (See Supplementary Information, Fig. S2) without evidence of a superconducting transition into the SC_1 phase down to 110 mK, well below its expected critical temperature, which usually ranges from 1.6 K to 2.1 K[2,3,5,9,29–32]. Disorder scattering, and thus approximate crystalline quality, is roughly estimated in metallic samples by dividing the resistivity at room temperature by the resistivity at 0 K (residual resistivity ratio: RRR = $\frac{R_{300K}(\Omega)}{R_{0K}(\Omega)}$), estimated in our case by extrapolating the T^2 fit 0-field data. Samples with a clear SC_1 transition show a great deal of variation in this regard, and can range from the typical[2] RRR = 18–40 all the way to a reported value of 1000 for exceptionally clean samples[29]. Little progress[27] has been made towards evaluating the relative sensitivities to disorder of the various superconducting phases, especially at high-fields.

UTe_2 crystals with no SC_1 transition usually have a RRR $\lesssim 5$, which implies a high degree of disorder[33,34]. While the value reported herein for Orphan UTe_2, RRR ≈ 7, is slightly out of this range, it still indicates that these samples are likewise quite disordered. To better understand the relative fragility of the low and high-field superconducting phases, we compare the extraordinarily robust oSC_{FP} phase diagram of Orphan UTe_2 with two additional crystals. For both additional crystals, $T_{cSC_1} \approx 1.85$ K, which indicates very good quality. However, the large variation of RRR values for "Low-R" (RRR = 8) and "High-R" (RRR = 64), crystals of low-field superconducting UTe_2 is atypical for any two superconductors with the same chemical formula and T_c value. This intimates that the scattering mechanisms that determine RRR in these samples are not identical to the determinants of T_c.

As shown in Fig. 1 and Fig. 2, the metamagnetic transition, H_m, occurs just below 35 T along the *b* axis in the Orphan UTe_2. This value is slightly lower than previous observations of H_m reported from low-field-superconducting samples of UTe_2[3,5,18,35–37], and lower than the metamagnetic transitions recorded for both Low-R and High-R UTe_2 (Fig. 2b). Nevertheless, the field value of this transition still corresponds to the temperature value of a maximum in the magnetic susceptibility with field along *b*, $T_\chi^{max} \approx 35$ K, previously reported for both nonsuperconducting[38] and superconducting[4] UTe_2. A similar feature is known in heavy fermion paramagnets with metamagnetic transitions, implying in those cases that H_m and T_χ^{max} are related by a single energy scale[39]. The agreement between the energy scales associated with T_χ^{max} and H_m is also important in UTe_2[13,35,36] and reflects the Kondo hybridization energy scale, as further observed in scanning tunneling microscopy[13] and magnetic excitations in inelastic neutron scattering experiments[40]. These results show that the heavy fermion state in UTe_2 is a robust characteristic.

We now consider the field-induced orphan superconducting phase that occurs at fields greater than H_m in the field polarized state. This oSC_{FP} phase, with boundaries defined here as 50% of the observed transition, emerges close to a 29° offset from *b* to *c* and extends to 42° (Fig. 1a). The narrower angular range of the oSC_{FP} is striking when compared to typical SC_{FP}, which extends from 25° to 42° in crystals with higher RRR (Fig. 2b, see Fig. S4 in Supplementary Information for comparison with published data[3,35,36,41]). Likewise, the field range oSC_{FP} is reduced, with an upper bound of 52 T. Previous reports have extrapolated the maximum field of SC_{FP} to above 65 T in samples with $T_{cSC_1} \approx 1.6$ K[3,5,25]. Nevertheless, in terms of magnetoresistance (Fig. 1), the transitions into the FP and SC_{FP} states are qualitatively similar to those in other samples. Note two important features: relatively wide transitions as a function of field and a limited range of zero resistance, both as measured at 0.5 K. The zero-resistance state is centered at 36°, which is far from the crystallographic (0 1 1) direction, situated at 23.7 °, suggesting that there is not a direct relationship between the two, which has been previously hypothesized[4].

The temperature dependence of oSC_{FP} gives further information about the unprecedented robustness of the superconductivity at these high-fields. The zero resistance state persists to just above 0.5 K (Fig. 3a), and a superconducting envelope persists to almost 0.9 K. All resistive signatures of superconductivity are suppressed by 1 K. This temperature differs dramatically from the value of 1.5 K reported before in samples exhibiting low field superconductivity[3], and even more so from the high T_{cSC_1} High-R sample (Fig. 3b). As shown in Fig. 3b, the critical temperature of a more-typical SC_{FP} phase is only slightly higher than that of the low field SC_1 phase. Previously, the similar T_c's reported for SC_1 and SC_{FP} led to the inference that the two phases must involve similar pairing energies[3], or even that SC_{FP} represents true reentrance of SC_1[42]. These observations led to the expectation that crystallographic disorder should affect T_c of both low-field and high-field superconductivity similarly. The observation of oSC_{FP} is at odds with this expectation, further suggesting that the scattering mechanism that dictates the values of RRR is not directly analogous to the strength of the superconducting pair-breaking that sets T_c.

Relevant theoretical attempts to describe high field superconductivity generally require the presence of zero-field

https://doi.org/10.1038/s41467-024-47090-1

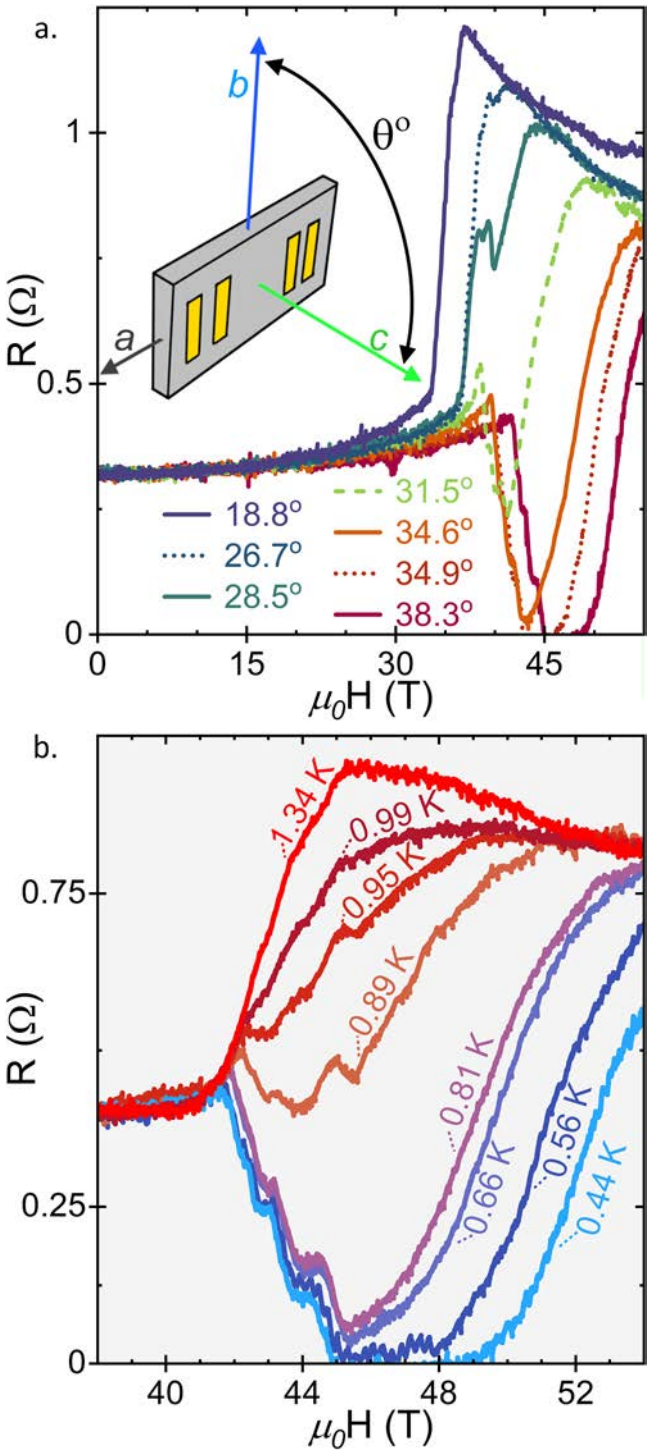

Fig. 1 | Magnetoresistance of orphan superconducting UTe_2 at select angles and base temperature, or at fixed angle and select temperatures. a Base temperature (~0.5 K) magnetoresistance (0 T < H < 55 T) of orphan superconducting UTe_2 at base temperature at select angles near the oSC_{FP} phase transition (angles are in degrees from crystallographic *b* to *c*). The large jumps in resistance near 35 T indicate the metamagnetic transition, H_m. Inset is an artistic render of the four-wire experimental setup with wires attached to four gold pads on the (001) sample face. **b** Magnetoresistance of orphan superconducting UTe_2 at with field applied at θ = 38.3° from *b* to *c*, measured at several temperatures from 1.34 K to base.

superconductivity[2,3,5,19–21,43], an assumption which has been reinforced by experimental evidence that high-field superconductivity is typically affected more strongly by temperature and disorder than low field superconductivity[26,44]. It is therefore surprising to see the presumptive fragile phase without its presupposedly more robust neighbor in Orphan UTe_2, and it will be instructive to review these mechanisms in light of the recontextualization demanded by the orphan SC_{FP} phase. The magnetic field dependence of the superconductivity due to these theoretical mechanisms is illustrated in Fig. 4.

Recently, the Jaccarino-Peter mechanism has been proposed as a likely candidate for the stabilization of SC_{FP} in UTe_2[25]. This mechanism is believed to be relevant to reentrant superconductivity in organic superconductors and several chevrel phases[45–47]. It involves an internal exchange field generated by the short-range magnetic fluctuations of localized moments, which opposes the applied magnetic field and reduces the total field[48], allowing superconductivity to persist to higher external fields than it otherwise should (Fig. 4). This exchange field can lead to reetrance, as in the Chevrel phase $Eu_{0.75}Sn_{0.25}Mo_6S_{7.2}Se_{0.8}$, in which zero-field superconductivity appears below 3.9 K and is suppressed by 1 T[45]. Above 4 T, the external field begins to adequately compensate for the internal exchange field, and superconductivity returns, persisting to approximately 22 T[45]. A similar mechanism is argued to be relevant to field-stabilized superconductivity in the antiferromagnetic insulator λ-$(BETS)_2FeCl_4$. Chemical substitution experiments show that the high-field range of the superconductivity is decreased when antiferromagnetism is destabilized and have been interpreted to indicate that λ-$(BETS)_2FeCl_4$ may have a "hidden" superconducting phase that competes with the antiferromagnetic internal field[49].

It was pointed out previously that the Jaccarino-Peter mechanism is likely not appropriate for UTe_2[3] because this effect requires localized moments and is typically observed in experiment over a narrow angular field range[48]. This contrasts sharply with the weak paramagnetic response of UTe_2, the substantial angular range of SC_{FP}, and the very large magnetic field scale. This inconsistency is reinforced by the new observations of Orphan SC_{FP}. The absence of zero field superconductivity without magnetic order to generate a negative exchange field at $H > 0$ almost entirely precludes the compensation-effect as the primary field-stabilizing mode in UTe_2

Another proposed explanation is that SC_{FP} is stabilized by ferromagnetic fluctuations[2], similar to field-reinforced superconductivity observed in ferromagnetic superconductors UCoGe[50] and URhGe[51] (Fig. 4). In this model, stabilizing longitudinal spin fluctuations arise near a second-order ferromagnetic transition driven by magnetic field[52]. Low field magnetometry measurements at ambient[38] and high pressure[53] imply that UTe_2 lies similarly at the cusp of magnetic order. However, UTe_2 strongly differs from the superconductors described by the spin-fluctuation model; these materials exhibit both long range magnetic order and low-field superconductivity which precede a field-reentrant superconducting phase[50,51] For example, spin fluctuations near a metamagnetic spin reorientation lead to reentrant superconductivity in URhGe, and strongly enhance T_{cRE} over the $H = 0$ critical temperature. The low field and reentrant superconducting transition temperatures in URhGe are highly sensitive to sample quality[26,54]. However, when the initial T_c boost from enhanced magnetic fluctuations near the metamagnetic field is accounted for, the ordering temperatures of the two phases are almost equally affected by disorder. In fact, the reentrant phase appears to be the slightly more fragile of the two[26].

Another mechanism for stabilizing high field superconductivity involves field-induced Landau level broadening near the quantum limit[43]. Mean field theory predicts that in applied fields strong enough to constrain electrons to the lowest Landau levels, T_c will increase in an oscillatory manner as a function of applied field, reflecting an enhancement of superconducting stability due to the Landau-level structure[43] (Fig. 4). It has even been hypothesized that approaching the extreme quantum limit could suppress the negative effects of disorder on T_c in the high-field regime[43]. Typically the field strength required for this is far beyond the Pauli limit for spin-singlet superconductors[43,55].

https://doi.org/10.1038/s41467-024-47090-1

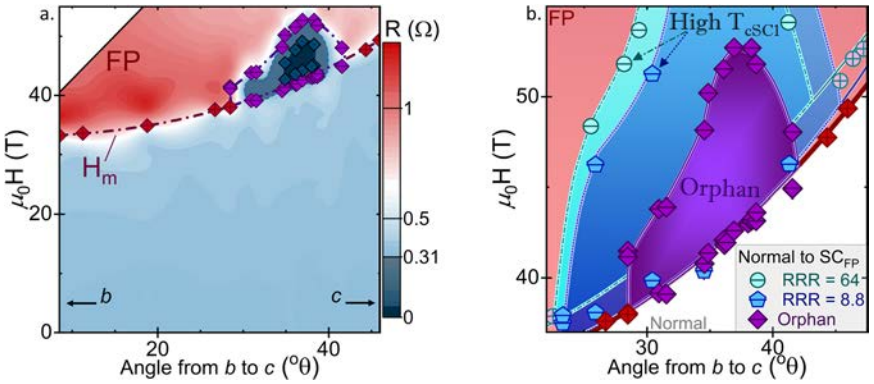

Fig. 2 | Field-Angle Phase Diagrams at Base Temperature. a Phase diagram of oSC_{FP} at base temperature (approx. 0.5 K), with color indicating total resistance. Circled dark blue regions between 30 and 44° are where the sample resistance falls below the average low field normal state value (~0.31 Ω) and the darkest color, bounded by dot-center diamonds, indicates zero resistance. Superconducting transitions and transitions from the low field normal to field polarized normal states (defined by 50% of the transition) are indicated by purple "-" crossed and red "+" crossed diamonds, respectively. **b** Comparison of the oSC_{FP} (purple "-" crossed) to SC_{FP} in $T_{cSC_1} \approx 1.85K$ RRR = 64 (- crossed circles) and RRR = 8.8 (- crossed pentagons) crystals between H = 35–55 T and θ = 20–50°. In all cases, the normal state (below H_m) is indicated in white, and the FP normal state (above Orphan UTe_2 H_m) in red. Best fit lines for each H_m and H_{c2} (dash-dot, short-dot, and solid for RRR = 64, 8.8, and Orphan UTe_2 crystals, respectively) are intended as guides to the eye.

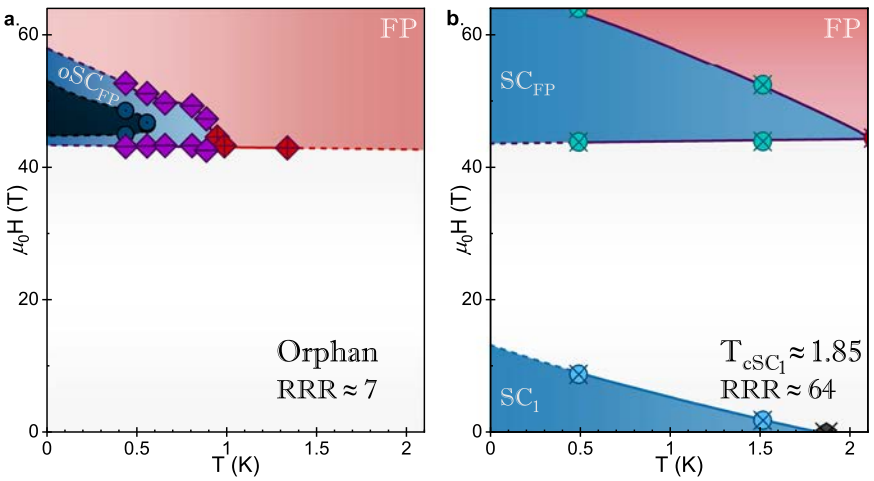

Fig. 3 | Comparison of Field-Temperature Phase Diagrams for Orphan Superconducting and High T_{cSC_1}, High RRR UTe_2. In both cases, the field polarized normal state (FP) is indicated in red, and regions of superconductivity (SC_1 at low field and SC_{FP} at high field) are in dark blue and bounded by lines (solid in between temperature points, dashed when extrapolating) intended as guides to the eye. See **Supplemental Information** for detailed information regarding the determination of phase boundaries and angles. **a** The field-temperature phase diagram of orphan high field superconductivity in Orphan UTe_2 at 38.3° offset between b and c. Points between which R = 0 Ω are designated with dark blue dotted circles, and the regions between temperature points have been interpolated a dashed-blue boarder and estimated to T = 0 K. Dashed lines between FP and either the low field normal state or SC_{FP} indicate regions where this boarder has been estimated to match scaling with **b**. Purple "-" crossed and red "+" crossed diamonds indicate 50% of resistive transitions between phases. **b** The field-temperature phase diagram of SC_{FP} in $T_{cSC_1} \approx 1.85K$, High-R crystal. Green and blue crossed circles indicate transitions to SC_1 and SC_{FP}, respectively as indicated by changes in PDO frequency (see **SI** for more detail). The 0 applied field T_{cSC_1}, indicated by a black crossed pentagon, was determined via four wire resistance in a Quantum Design Physical Properties Measurement System.

Landau-level stabilized superconductivity is therefore most likely to be realized in spin-triplet superconductors. Indeed, high pressure measurements of resistance in low-field-superconducting UTe_2 show possible precursor effects quantized with the signature 1/H relation to SC_1 and SC_{FP}[22]. However, this model is not without controversy: it has been argued that "unless the [Landé] g-factor is exactly 0[56]," which is not true in UTe_2[27], "re-entrant superconductivity can be expected only if there is a superconducting transition in zero field[56]." Moreover, a low-dimensional electronic structure is usually assumed for models of superconductivity near the quantum limit[43], and such a structure could not be inferred in UTe_2 from angle-resolved photoemission spectroscopy[57]. Recent de Haas van Alphen oscillation measurements of low-field superconducting UTe_2 suggest quasi-two-dimensional cylindrical electron and hole Fermi surface sections[58]. However, the Fermi surface has three-dimensional characteristics[59–61], and the inverse-field periodicity implies a small orbit that has yet to be conclusively demonstrated. A separate theoretical analysis has proposed that SC_{FP} in UTe_2 may be stabilized near the quantum limit by a Hofstadter butterfly regime of Landau level quantization with large superlattices[62]. This stabilization regime would, if accurate, indicate the existence of an even higher field phase beyond SC_{FP}, located at approximately 90 T[22,62], and moreover that the quantum limit field has somehow been lowered from the H > 100 T region inferred from recently reported[59,60] quantum oscillation frequencies. Furthermore, confirmation of this model would ideally involve observation of superconductivity in multiple Landau levels, requiring challenging measurements performed at significantly higher magnetic fields.

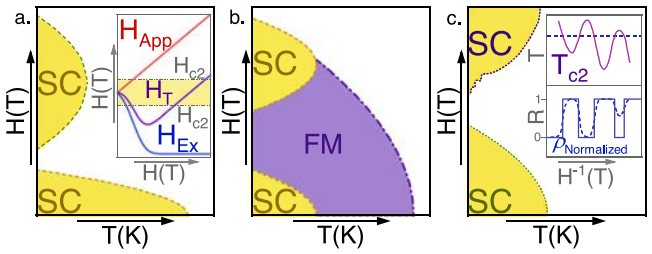

Fig. 4 | Magnetic field–temperature schematic phase diagrams for superconductivity stabilized by different possible mechanisms. a The Jaccarino-Peter compensation effect. An internal exchange field (H_{Ex}, blue) opposes the applied field (H_{App}) resulting in reentrant superconductivity when the total internal field (H_T, purple) is smaller than H_{c2}. **b** Stabilization of ferromagnetic superconductivity near a quantum critical point. Strong magnetic fluctuations due to the destabilization of long-range magnetism enhance the superconducting pairing. Superconductivity can survive at and on either side of the QCP. **c** Superconductivity stabilized near the quantum limit. The upper critical field of reentrant superconductivity in this case is oscillatory in inverse field.

The above inconsistencies show that SC_{FP} is likely not a field-stabilized version of SC_1 and its pairing state should be considered separately. In other words, SC_{FP} and SC_1 are substantially different superconducting phases, could involve different superconducting pairing mechanisms, and their gap structure and size are different. The lack of a parent superconducting instability makes it more remarkable that SC_{FP} is stable at such high magnetic fields, as the dominant theoretical descriptions of high-field superconductivity presuppose a low-field antecedent. While none of the three scenarios we have discussed anticipate oSC_{FP}, other potential explanations such as the invocation of "hidden" superconductivity in UTe_2, similar to that in the Chevrel[47] case, would require even more a priori assumptions and cannot be considered useful models at this stage. We must conclude that further understanding of SC_{FP} specifically, and field stabilized superconductivity as a whole, demand the further development of models of high-field superconductivity that do not evolve from a low field superconducting phase.

Methods

All samples were grown as single crystals via chemical vapor transport with iodine oas the transport agent. Orphan UTe_2 crystals were grown over one week as thin plates approximately 3 mm in length from a 2:3 U:Te ratio in a two zone furnace set to 800 °C and 710 °C in the charge and growth zones, respectively. The Low-R and High-R samples were grown in a two zone furnace at 900 °C (charge zone) and 830 °C (growth zone) over two weeks with starting U:Te ratios of 5:9 and 2:3, respectively. At the end of the growth period, transport was quenched by turning off power to the heating elements. Crystallographic orientation was identified from the crystal habit.

Zero-field resistance measurements to 100 mK were performed on a Quantum Design Physical Property Measurement System (PPMS) using the adiabatic demagnetization refrigerator (ADR) option. For high field measurements, crystals were mounted on a cryogenic single axis goniometer[63] at the National High Magnetic Field Laboratory (NHMFL), Los Alamos, NM and rotated between the (010) and (001) faces at applied fields of up to 55 T or up to 60 T. Both high field magnetoresistance and proximity diode oscillator measurements were performed using a 65 T short-pulse magnet. Identification of commercial equipment does not imply recommendation or endorsement by NIST.

Data availability

The phase boundaries represented in Figs. 1–3 are available as tables and their definitions explained in detail in the Supplementary Information. Raw magnetoresistance and PDO data files are publicly available in the OSF Repository: https://doi.org/10.17605/OSF.IO/Q3HSE[64]. All other data are available from the corresponding authors upon request.

References

1. Aoki, D., Ishida, K. & Flouquet, J. Review of U-based ferromagnetic superconductors: comparison between UGe_2, URhGe, and UCoGe. *J. Phys. Soc. Jpn.* **88**, 022001 (2019).
2. Ran, S. et al. Nearly ferromagnetic spin-triplet superconductivity. *Science* **365**, 684–687 (2019).
3. Ran, S. et al. Extreme magnetic field-boosted superconductivity. *Nat. Phys.* **15**, 1250–1254 (2019).
4. Knafo, W. et al. Comparison of two superconducting phases induced by a magnetic field in UTe_2. *Commun. Phys.* **4**, 40 (2021).
5. Aoki, D. et al. Unconventional superconductivity in UTe_2. *J. Phys. Condens. Matter* **34**, 243002 (2022).
6. Hayes, I. M. et al. Multicomponent superconducting order parameter in UTe_2. *Science* **373**, 797–801 (2021).
7. Fujibayashi, H. et al. Superconducting order parameter in UTe_2 determined by knight shift measurement. *J. Phys. Soc. Jpn.* **91**, 043705 (2022).
8. Shishidou, T., Suh, H. G., Brydon, P. M. R., Weinert, M. & Agterberg, D. F. Topological band and superconductivity in UTe_2. *Phys. Rev. B* **103**, 104504 (2021).
9. Thomas, S. M. et al. Spatially inhomogeneous superconductivity in UTe_2. *Phys. Rev. B* **104**, 224501 (2021).
10. Ajeesh, M. O. et al. Fate of time-reversal symmetry breaking in UTe_2. *Phys. Rev. X* **13**, 041019 (2023).
11. Florian, T. et al. Resonant Ultrasound Spectroscopy for Irregularly Shaped Samples and Its Application to Uranium Ditelluride. *Phys. Rev. Lett.* **132**, 066003 (2024).
12. Ishihara, K. et al. Chiral superconductivity in UTe2 probed by anisotropic low-energy excitations. *Nat. Commun.* **14**, 2966 (2023).
13. Jiao, L. et al. Chiral superconductivity in heavy-fermion metal UTe_2. *Nature* **579**, 523–527 (2020).
14. Bae, S. et al. Anomalous normal fluid response in a chiral superconductor UTe2. *Nat. Commun.* **12**, 2644 (2021).
15. Matsumura, H. et al. Large reduction in the a-axis Knight Shift on UTe2 with Tc = 2.1 K. *J. Phys. Soc. Jpn.* **92**, 063701 (2023).
16. Nakamine, G. et al. Inhomogeneous superconducting state probed by 125Te NMR on UTe2. *J. Phys. Soc. Jpn.* **90**, 064709 (2021).
17. Sakai, H. et al. Field induced multiple superconducting phases in UTe_2 along hard magnetic axis. *Phys. Rev. Lett.* **130**, 196002 (2023).
18. Rosuel, A. et al. Field-induced tuning of the pairing state in a superconductor. *Phys. Rev. X* **13**, 011022 (2023).
19. Kazushige, M. Violation of the orbital depairing limit in a nonunitary state: High-field phase in the heavy fermion superconductor UTe_2. *Phys. Rev. B* **107**, 224512 (2023).
20. Mineev, V. P. Reentrant superconductivity in UTe_2. *J. Exp. Theor. Phys. Lett.* **111**, 715–719 (2020).
21. Lebed, A. G. Restoration of superconductivity in high magnetic fields in UTe_2. *Mod. Phys. Lett. B* **34**, 2030007 (2020).
22. Ran, S. et al. Expansion of the high field-boosted superconductivity in UTe_2 under pressure. *npj Quantum Mater.* **6**, 75 (2021).
23. Knebel, G. et al. Anisotropy of the upper critical field in the heavy-fermion superconductor UTe2 under pressure. *J. Phys. Soc. Jpn.* **89**, 053707 (2020).
24. Aoki, D. et al. Field-induced superconductivity near the superconducting critical pressure in UTe_2. *J. Phys. Soc. Jpn.* **90**, 074705 (2021).
25. Helm, T. et al. Field-induced compensation of magnetic exchange as the possible origin of reentrant superconductivity in UTe_2. *Nat. Commun.* https://doi.org/10.1038/s41467-023-44183-1 (2024).

26. Miyake, A., Aoki, D. & Flouquet, J. Field re-entrant superconductivity induced by the enhancement of effective mass in URhGe. *J. Phys. Soc. Jpn.* **77**, 094709 (2008).
27. Wu, Z. et al. Enhanced triplet superconductivity in next generation ultraclean UTe2. Preprint at https://doi.org/10.48550/arXiv.2305.19033 (2023).
28. Ishihara, K. et al. Anisotropic enhancement of lower critical field in ultraclean crystals of spin-triplet superconductor candidate UTe 2. *Phys. Rev. Res.* **5**, L022002 (2023).
29. Sakai, H. et al. Single crystal growth of superconducting UTe_2 by molten salt flux method. *Phys. Rev. Mater.* **6**, 073401 (2022).
30. Aoki, D. et al. Multiple superconducting phases and unusual enhancement of the upper critical field in UTe_2. *J. Phys. Soc. Jpn.* **89**, 053705 (2020).
31. Braithwaite, D. et al. Multiple superconducting phases in a nearly ferromagnetic system. *Commun. Phys.* **2**, 147 (2019).
32. Sundar, S. et al. Coexistence of ferromagnetic fluctuations and superconductivity in the actinide superconductor UTe_2. *Phys. Rev. B* **100**, https://doi.org/10.1103/physrevb.100.140502 (2019).
33. Ran, S. et al. Comparison of two different synthesis methods of single crystals of superconducting uranium ditelluride. *J. Vis. Exp.* **173**, e62563 (2021).
34. Rosa, P. F. S. et al. Single thermodynamic transition at 2 K in superconducting UTe_2 single crystals. *Commun. Mater.* **3**, 33 (2022).
35. Miyake, A. et al. Metamagnetic transition in heavy fermion superconductor UTe_2. *J. Phys. Soc. Jpn.* **88**, 063706 (2019).
36. Niu, Q. et al. Evidence of Fermi surface reconstruction at the metamagnetic transition of the strongly correlated superconductor UTe_2. *Phys. Rev. Res.* **2**, 033179 (2020).
37. Miyake, A. et al. Enhancement and discontinuity of effective mass through the first-order metamagnetic transition in UTe_2. *J. Phys. Soc. Jpn.* **90**, 103702 (2021).
38. Ikeda, S. et al. Single crystal growth and magnetic properties of UTe_2. *J. Phys. Soc. Jpn.* **75**, 116–118 (2006).
39. Aoki, D., Knafo, W. & Sheikin, I. Heavy fermions in a high magnetic field. *Comptes Rendus Phys.* **14**, 53–77 (2013).
40. Butch, N. P. et al. Symmetry of magnetic correlations in spin-triplet superconductor UTe_2. *npj Quantum Mater.* **7**, 39 (2022).
41. Knebel, G. et al. Field-reentrant superconductivity close to a metamagnetic transition in the heavy-fermion superconductor UTe_2. *J. Phys. Soc. Jpn.* **88**, 063707 (2019).
42. Machida, K. Nonunitary triplet superconductivity tuned by field-controlled magnetization: URhGe, UCoGe, and UTe_2. *Phys. Rev. B* **104**, 014514 (2021).
43. Rasolt, M. & Tešanović, Z. Theoretical aspects of superconductivity in very high magnetic fields. *Rev. Mod. Phys.* **64**, 709 (1992).
44. Aoki, D. et al. Spin fluctuation and Fermi surface instability in ferromagnetic superconductors. *Comptes Rendus Phys.* **15**, 630–639 (2014).
45. Meul, H. et al. Observation of magnetic-field-induced superconductivity. *Phys. Rev. Lett.* **53**, 497 (1984).
46. Burlet, P. et al. Magnetism and superconductivity in the Chevrel phase $HoMo_6S_8$. *Phys. B Condens. Matter* **215**, 127–133 (1995).
47. Hiraki, K. I. et al. ^{77}Se NMR evidence for the Jaccarino–Peter mechanism in the field induced superconductor, λ-$(BETS)_2FeCl_4$. *J. Phys. Soc. Jpn.* **76**, 124708 (2007).
48. Hampshire, D. P. In *Handbook of Superconductivity* 178-202 (CRC Press, 2023).
49. Uji, S. & S. Brooks, J. Magnetic-field-induced superconductivity in organic conductors. *J. Phys. Soc. Jpn.* **75**, 051014 (2006).
50. Huy, N. et al. Superconductivity on the border of weak itinerant ferromagnetism in UCoGe. *Phys. Rev. Lett.* **99**, 067006 (2007).
51. Aoki, D. et al. Coexistence of superconductivity and ferromagnetism in URhGe. *Nature* **413**, 613–616 (2001).
52. Slooten, E., Naka, T., Gasparini, A., Huang, Y. K. & de Visser, A. Enhancement of superconductivity near the ferromagnetic quantum critical point in UCoGe. *Phys. Rev. Lett.* **103**, 097003 (2009).
53. Li, D. et al. Magnetic properties under pressure in novel spin-triplet superconductor UTe_2. *J. Phys. Soc. Jpn.* **90**, 073703 (2021).
54. Lévy, F., Sheikin, I., Grenier, B. & Huxley, A. D. Magnetic field-induced superconductivity in the ferromagnet URhGe. *Science* **309**, 1343–1346 (2005).
55. Gruenberg, L. & Gunther, L. Effect of orbital quantization on the critical field of type-II superconductors. *Phys. Rev.* **176**, 606 (1968).
56. Rieck, C. T., Scharnberg, K. & Klemm, R. A. Re-entrant superconductivity due to Landau level quantization? *Phys. C Supercond.* **170**, 195–210 (1990).
57. Miao, L. et al. Low energy band structure and symmetries of UTe_2 from angle-resolved photoemission spectroscopy. *Phys. Rev. Lett.* **124**, 076401 (2020).
58. Aoki, D. et al. First observation of the de Haas–van Alphen effect and Fermi surfaces in the unconventional superconductor UTe_2. *J. Phys. Soc. Jpn.* **91**, 083704 (2022).
59. Eaton, A. et al. Quasi-2D Fermi surface in the anomalous superconductor UTe_2. *Nat. Commun.* **15**, 223 (2024).
60. Christopher, B. et al. Revealing a 3D Fermi Surface and Electron-Hole Tunneling in UTe_2 with Quantum Oscillations. *Phys. Rev. Lett.* **131**, 036501 (2023).
61. Eo, Y. S. et al. c-axis transport inUTe_2: Evidence of three-dimensional conductivity component. *Phys. Rev. B* **106**, L060505 (2022).
62. Park, M. J., Kim, Y. B. & Lee, S. Geometric superconductivity in 3d Hofstadter butterfly. Preprint at https://doi.org/10.48550/arXiv.2007.16205 (2020).
63. Willis, X., Ding, X., Singleton, J. & Balakirev, F. F. Cryogenic goniometer for measurements in pulsed magnetic fields fabricated via additive manufacturing technique. *Rev. Sci. Instrum.* **91**, 036102 (2020).
64. Frank, C. E. et al. *Data for "Orphan high field superconductivity in non-superconducting uranium ditelluride."* https://doi.org/10.17605/OSF.IO/Q3HSE (2024).

Acknowledgements

This work was supported in part by the National Science Foundation under the Division of Materials Research Grant NSF-DMR 2105191 (synthesis and high field experiments), the Department of Energy Award No. DE-SC-0019154 (sample characterization) the Gordon and Betty Moore Foundation's EPiQS Initiative through Grant No. GBMF9071 (materials synthesis), and the Maryland Quantum Materials Center. A portion of this work was performed at the National High Magnetic Field Laboratory (NHMFL), which is supported by National Science Foundation Cooperative Agreements DMR-1644779 and DMR-2128556, and the Department of Energy (DOE). JS acknowledges support from the DOE BES program "Science of 100 T", which permitted the design and construction of much of the specialized equipment used in the high-field studies. The authors would like to express their gratitude to University of Maryland undergraduate students: Patrick Chen, Elan Moskowitz, and Kimia Samieninejad, for their assistance in pulsed field measurement preparations.

Author contributions

N.P.B. directed the project. C.E.F synthesized single crystalline samples. C.E.F., G.S.S., and S.K.L. oriented and prepared samples for magnetoresistance measurements. C.E.F, S.K.L, and J.S. performed the magnetoresistance measurements in the pulsed field. C.E.F. performed resistivity measurements at zero field. I.H., T.M., and H.Y. performed preliminary measurements. J.P. and P.C. contributed to data analysis. C.E.F. and N.P.B. wrote the manuscript with contributions from all authors.

Competing interests
The authors declare no competing interests.

Additional information
Supplementary information The online version contains supplementary material available at https://doi.org/10.1038/s41467-024-47090-1.

Correspondence and requests for materials should be addressed to Corey E. Frank or Nicholas P. Butch.

Peer review information *Nature Communications* thanks the anonymous, reviewer(s) for their contribution to the peer review of this work. A peer review file is available.

Orphan High Field Superconductivity in Non-Superconducting Uranium Ditelluride

Supplementary Information

Corey E. Frank,[1,2*] Sylvia K. Lewin,[1,2] Gicela Saucedo Salas,[2,1] Peter Czajka,[1,2] Ian M. Hayes,[2] Hyeok Yoon,[2] Tristin Metz,[2] Johnpierre Paglione,[2,3] John Singleton,[4] Nicholas P. Butch[1,2*]

1. NIST Center for Neutron Research, National Institute of Standards and Technology, Gaithersburg, MD, USA
2. Maryland Quantum Materials Center, Department of Physics, University of Maryland, College Park, MD, USA
3. Canadian Institute for Advanced Research, Toronto, Ontario M5G 1Z8, Canada
4. National High Magnetic Field Laboratory, Los Alamos National Laboratory, Los Alamos, NM, USA

**To whom correspondence should be addressed.*

Sample Preparation and Resistivity Measurements at 0 T applied Magnetic Field

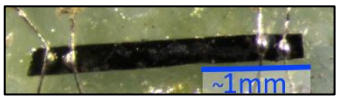

Figure S 1 Approx. 2.5 mm crystal of low-field non superconducting UTe_2 grown as a flat plate in the *ab* plane via chemical vapor transport, as described in main text. Crystal is depicted with typical four-wire configuration as used for resistance measurements.

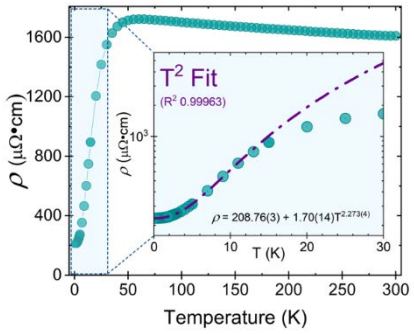

Figure S 2 Preliminary, zero field resistance of the specially prepared low-field non-superconducting UTe_2 sample used for high field magnetoresistance measurements at NHMFL Pulsed Field Facility. At applied field H = 0 T, this sample showed no indication of a superconducting transition to 0.110 K . A T^2 fit of the resistance indicates Fermi-liquid behavior to approximately 10 K, a two order of magnitude range.

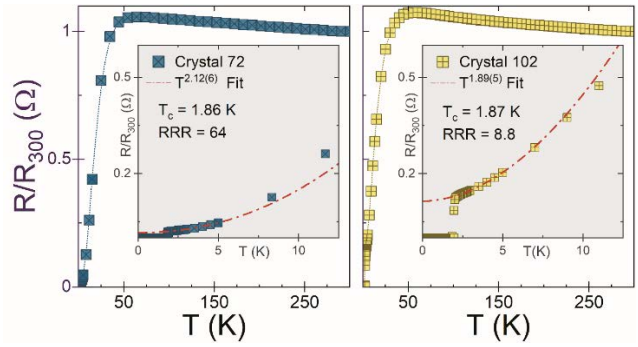

Figure S 3 Preliminary, zero field resistance of high T_c UTe_2 samples used for high field proximity diode oscillator measurements at NHMFL Pulsed Field Facility.

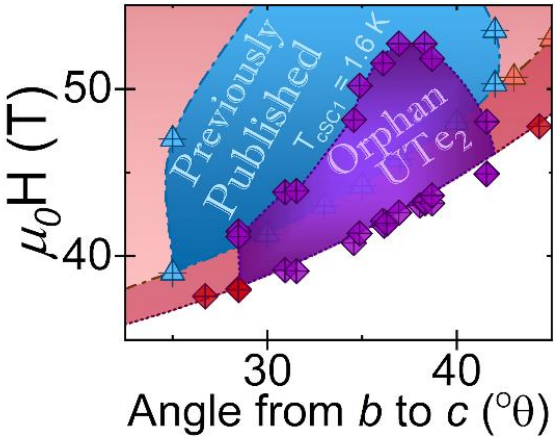

Figure S 4. Phase diagram of resistance in applied field (y-axis) vs angular offset from *b* to *c* for orphan-superconducting UTe_2. Superconducting transitions (defined by 50% of the transition) are shown in purple diamonds, and transitions from the low-field-normal state to the field-polarized-normal state are indicated by red diamonds. The orphan superconducting region is indicated in purple and the field polarized normal state in red, with colors and lines as a guide to the eye. The dashed red line is a fit of H_m in orphan UTe_2, also intended as a guide to the eye. These data are overlayed with previously reported[1] data. Referenced UTe_2 phase boundaries are shown as simple, smooth blue lines for clarity and are intended as a tool of contextualization. Solid blue regions indicate superconductivity in archetypical ($T_{c_{SC1}} \approx 1.6$ K) UTe_2 only, and the solid red region indicates the angular range of the field polarized regime in the *bc* plane.[1]

Data Processing and Definition of Phase Boundaries – Orphan UTe_2

For phase diagrams shown in the main text, transitions were defined as 50% of the difference in resistance between the normal and field polarized, the normal and superconducting, or the superconducting and field polarized states, respectively. To define transitions from the normal state or superconducting states to the field polarized regime, or from the normal state to oSC_{FP}, a point was chosen where resistance was a relative minimum (R_{min}) proximal to the inflection point. For a full superconducting transition, $R_{min} = 0$ Ω. The point of maximum resistance, R_{max}, after (before) this transition defines the normal state resistance in the FP (before the oSC_{FP}) phaseOnce the limits were defined, the 10%, 50%, and 90% resistance values between them were calculated, and the corresponding applied field values found on each curve (**Fig S.5**). These values are listed in the tables below. In cases where the maximum value of resistance fell outside of the measured value for the respective field pulse, R_{max} was estimated. This estimation was performed by plotting R_{max} vs angle for well-defined pulses as can be seen in **Fig S.6**. Data were combined with data from Fig 1 in the main text to generate Fig 2 in the main text.

[1] Ran, S. *et al.* Extreme magnetic field-boosted superconductivity. *Nature Physics* **15**, 1250-1254, doi:10.1038/s41567-019-0670-x (2019).

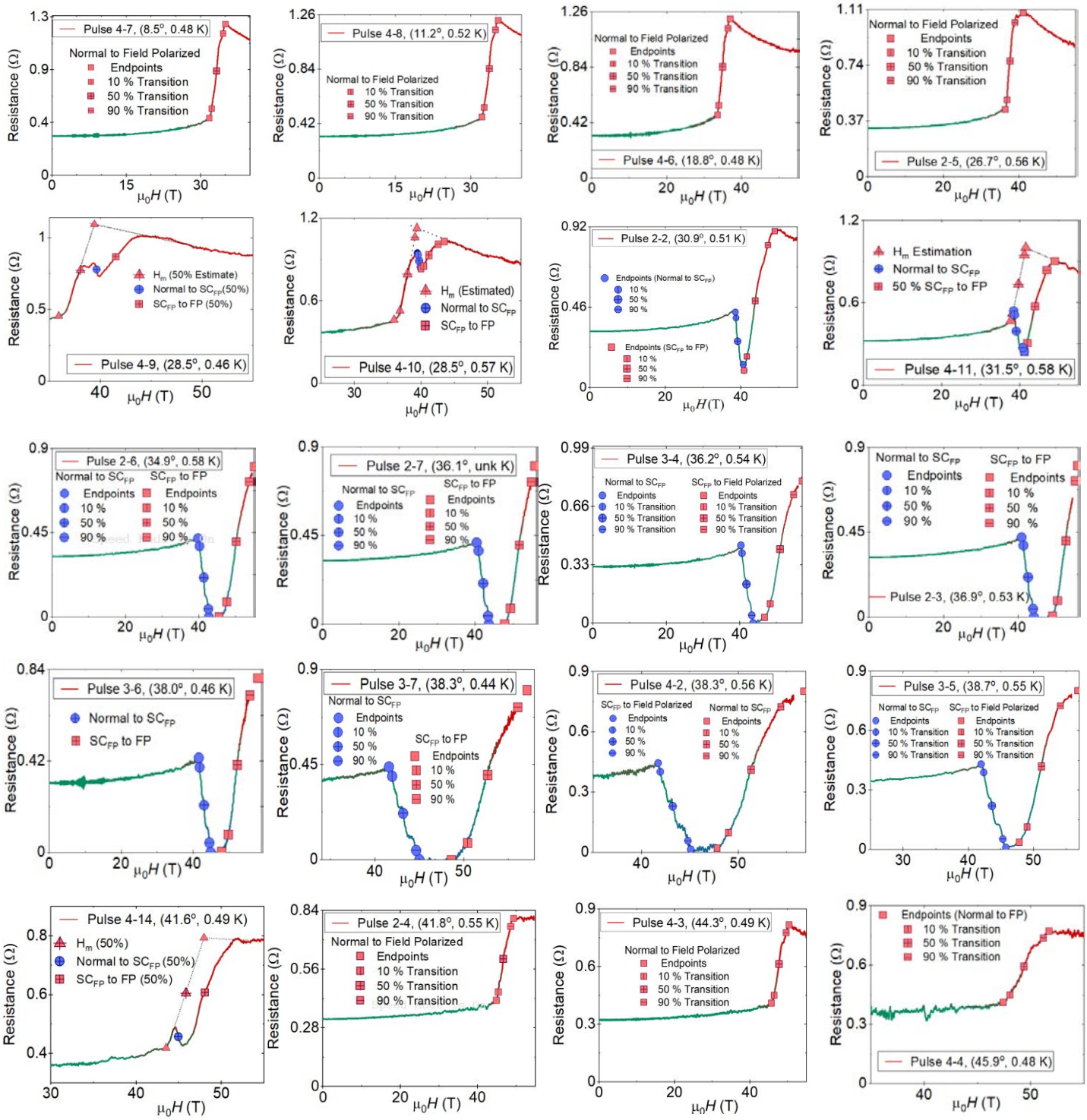

Figure S 5 Base-temperature resistance curves showing a transition to the field polarized state (red squares), from the normal state to oSC$_{FP}$ (blue circles), and in some cases an estimation of H_m when interrupted by a partial superconducting transition (red triangles). The interior of each shape indicates the endpoints (open shapes), 10 % (vertical center line), 50 % (crosses), and 90 % (horizontal crosses) points of the respective transitions. Resistance curves shown here are from the pulsed field magnet downsweep only. Data used to construct Fig. 1 in the main text.

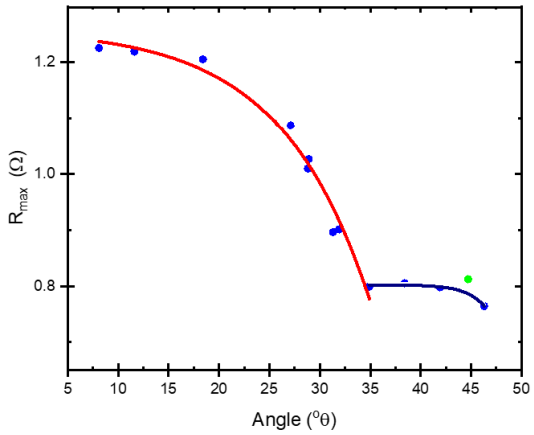

Figure S 6 Maximum resistance (Ohms) of base temperature magnetoresistance measurements vs field angle (degrees from *b* to *c*). Fitting angle vs R_{max} allows for R_{max} to be estimated when R_{max} is outside of measurement range.

Temperature Dependent Measurements on Orphan UTe_2 at θ = 38.3° between *b* and *c*.

Table S. 1 Temperature Dependent H_m (Low Field Normal State to oSC_{FP})

Temp (K)	**Angle θ (°)**	Starting Values		End Values		**50% Transition**		90% Transition		10% Transition	
		μ_0H (T)	R (Ω)	μ_0H (T)	R (Ω)	**μ_0H (T)**	R (Ω)	μ_0H (T)	R (Ω)	μ_0H (T)	R (Ω)
0.44	**38.3**	41.6	0.4386	45.0	0	**43.2**	0.2193	44.6	0.0439	41.9	0.3948
0.56	**38.3**	41.7	0.4367	45.2	0.0113	**43.3**	0.224	44.8	0.0539	42.0	0.3941
0.66	**38.3**	41.8	0.4627	45.5	0.0367	**43.3**	0.2497	45.0	0.0793	42.1	0.4201
0.81	**38.3**	41.8	0.4635	45.4	0.0572	**43.3**	0.2603	44.9	0.0978	42.1	0.4229
0.95	**38.3**	41.2	0.4394	49.4	0.8384	**44.6**	0.6389	47.9	0.7985	41.9	0.4793

Transitions (as defined above) from the low-field normal state into oSC_{FP} at varying temperatures and constant angle. Data used to construct Fig. 2 in the main text.

Table S. 2 Temperature Dependent H_m or H_{C2} (Low Field Normal or oSC_{FP} to Field Polarized Normal State)

Temp (K)	**Angle θ (°)**	Starting Values		End Values		**50% Transition**		90% Transition		10% Transition	
		μ_0H (T)	R (Ω)	μ_0H (T)	R (Ω)	**μ_0H (T)**	R (Ω)	μ_0H (T)	R (Ω)	μ_0H (T)	R (Ω)
0.44	**38.3**	48.6	0	51.8	0.8026	**52.7**	0.4013	57.1	0.7224	50.4	0.0803
0.56	**38.3**	48.1	0.0294	54.8	0.7538	**51.2**	0.3916	53.8	0.6814	49.0	0.1019
0.66	**38.3**	45.5	0.0367	54.5	0.7816	**49.7**	0.4091	52.3	0.7071	47.3	0.1112
0.81	**38.3**	45.4	0.0572	54.7	0.8059	**49.3**	0.4315	52.1	0.731	46.9	0.132
0.89	**38.3**	43.9	0.4085	51.2	0.8368	**47.3**	0.6227	50.2	0.794	44.5	0.4513
0.99	**38.3**	40.8	0.4144	48.6	0.8525	**43.3**	0.6334	45.6	0.8087	41.6	0.4582
1.34	**38.3**	40.8	0.4146	45.5	0.9483	**43.0**	0.6815	44.7	0.8949	41.7	0.468

Transitions (as defined above) from the low-field normal state or oSC_{FP} into the field polarized normal state at varying temperatures and constant angle. Data used to construct Fig. 2 in the main text.

Angle Dependent Measurements on Orphan UTe_2 at Base Temperature

Table S. 3 Angle Dependent H_m (Low Field Normal State to oSC_{FP}) for Orphan UTe_2

Temp (K)	**Angle θ (º)**	Starting Values μ_0H (T)	Starting Values R (Ω)	End Values μ_0H (T)	End Values R (Ω)	**50% Transition μ_0H (T)**	**50% Transition R (Ω)**	90% Transition μ_0H (T)	90% Transition R (Ω)	10% Transition μ_0H (T)	10% Transition R (Ω)
0.46	**28.5**	39.4	0.8224	39.7	0.7372	**39.6**	0.7798	39.7	0.7457	39.5	0.8138
0.57	**28.5**	39.4	0.9452	40	0.8347	**39.7**	0.8899	39.9	0.8457	39.6	0.9341
0.51	**30.9**	38.6	0.4322	40.9	0.0982	**39.2**	0.2652	40.6	0.1316	38.7	0.3988
0.58	**31.5**	38.4	0.5404	41.2	0.2423	**39.1**	0.3914	40.8	0.2721	38.7	0.5106
0.57	**34.6**	39.6	0.4758	42.6	0.0376	**40.8**	0.2567	42.3	0.0814	39.8	0.432
0.58	**34.9**	39.8	0.4195	42.7	0	**41.4**	0.2097	42.6	0.0419	40.2	0.3775
unk	**36.1**	40.4	0.4131	43.6	0	**42.1**	0.2066	43.4	0.0413	40.9	0.3718
0.54	**36.2**	40.3	0.439	43.7	0	**41.8**	0.2195	43.3	0.0439	40.6	0.3951
0.59	**36.3**	40.5	0.4573	43.8	0.0222	**42**	0.2398	43.4	0.0657	40.8	0.4138
0.53	**36.9**	40.9	0.4214	44.2	0	**42.6**	0.2107	44	0.0421	41.4	0.3793
0.46	**38**	41.6	0.4338	44.9	0	**43**	0.2169	44.5	0.0434	41.8	0.3904
0.44	**38.3**	41.6	0.4386	45	0	**43.2**	0.2193	44.6	0.0439	41.9	0.3948
0.56	**38.3**	41.7	0.4437	45.1	0.0144	**43.2**	0.2291	44.8	0.0573	42	0.4008
0.48	**38.7**	41.8	0.4957	45.2	0.0746	**43.2**	0.2852	44.9	0.1167	42	0.4536
0.55	**38.7**	42	0.4304	45.7	0.0099	**43.6**	0.2201	45.3	0.0519	42.4	0.3883
0.49	**41.6**	44.6	0.4887	45.5	0.4263	**44.9**	0.4575	45.3	0.4326	44.7	0.4825

Transitions (as defined above) from the low-field normal state into oSC_{FP} at varying angles from *b* to *c* and base temperature (approximately 500 mK). Data used to construct Fig. 1 in the main text.

Table S. 4 Angle Dependent H_{C2} (oSC_{FP} to Field Polarized Normal State) for Orphan UTe_2*

Temp (K)	**Angle θ (º)**	Starting Values μ_0H (T)	Starting Values R (Ω)	End Values μ_0H (T)	End Values R (Ω)	**50% Transition μ_0H (T)**	**50% Transition R (Ω)**	90% Transition μ_0H (T)	90% Transition R (Ω)	10% Transition μ_0H (T)	10% Transition R (Ω)
0.46	**28.5**	39.9	0.7293	43.8	1.008	**41.5**	0.8686	42.9	0.9801	40.2	0.7572
0.57	**28.5**	40	0.8347	43.5	1.0312	**41.2**	0.933	42.6	1.0116	40.4	0.8543
0.51	**30.9**	40.9	0.0982	49	0.8946	**43.8**	0.4964	47.2	0.815	41.6	0.1778
0.58	**31.5**	41.2	0.2423	49	0.904	**43.9**	0.5732	46.9	0.8379	41.9	0.3085
0.57	**34.6**	43.2	0.0319	53.9	0.7945	**48.2**	0.4132	51.7	0.7183	44.8	0.1082
0.58	**34.9**	45.5	0	Estimated	0.8031	**50.2**	0.4016	53.8	0.7228	47.6	0.0803
unk	**36.1**	47.7	0	Estimated	0.803	**51.5**	0.4015	54.7	0.7227	49.2	0.0803
0.54	**36.2**	46.7	0.032	Estimated	0.803	**51**	0.4175	54.7	0.7259	48.3	0.1091
0.59	**36.3**	45.9	0.0335	Estimated	0.803	**50.3**	0.4182	53.8	0.7261	47.5	0.1104
0.53	**36.9**	49.1	0.007	Estimated	0.8029	**52.7**	0.405	55.2	0.7233	50.4	0.0866
0.46	**38**	47.9	0.0025	Estimated	0.8027	**52.3**	0.4026	55.7	0.7227	49.7	0.0825
0.44	**38.3**	48.6	0	Estimated	0.8026	**52.7**	0.4013	56.1	0.7224	50.4	0.0803
0.56	**38.3**	47.8	0.0213	Estimated	0.8026	**51.3**	0.4119	54.4	0.7245	49	0.0994
0.48	**38.7**	48.7	0.1146	Estimated	0.8731	**51.8**	0.4938	54.5	0.7972	49.7	0.1904
0.55	**38.7**	47.8	0.0375	Estimated	0.8025	**51.2**	0.42	54	0.726	49	0.114
0.49	**41.6**	43.5	0.4186	51.8	0.7902	**48**	0.6083	50.6	0.7539	46.6	0.4627

Transitions (as defined above) from SC_{FP} into the field polarized normal state at varying angles from *b* to *c* and base temperature (approximately 500 mK). Data used to construct Fig. 1 in the main text. Estimation of H_{max} from utilized where "fitting function" is listed in the table.

Table S. 5 Angle Dependent H_m (Low Field to Field Polarized Normal State) for Orphan UTe_2

Temp (K)	**Angle θ (°)**	Starting Values $\mu_0 H$ (T)	Starting Values R (Ω)	End Values $\mu_0 H$ (T)	End Values R (Ω)	**50% Transition $\mu_0 H$ (T)**	**50% Transition R (Ω)**	90% Transition $\mu_0 H$ (T)	90% Transition R (Ω)	10% Transition $\mu_0 H$ (T)	10% Transition R (Ω)
0.48	**8.5**	31.7	0.4699	35	1.2319	**33.2**	0.8509	34.5	1.1557	32.2	0.5461
0.52	**11.2**	32.1	0.4711	35.4	1.219	**33.6**	0.8451	34.9	1.1442	32.6	0.5459
0.48	**18.8**	33.5	0.4802	36.9	1.2064	**34.9**	0.8433	36.3	1.1337	33.9	0.5528
0.56	**26.7**	36.3	0.4473	41.1	1.0893	**37.6**	0.7683	38.9	1.0251	36.8	0.5115
0.46	**28.5**	35.9	0.4545	39.4	1.0932	**38**	0.7739	39.1	1.0294	36.8	0.5184
0.57	**28.5**	36	0.4613	39.4	1.1282	**38**	0.7948	39.1	1.0615	36.9	0.528
0.58	**41.6**	43.3	0.4118	47.1	0.8263	**45.5**	0.619	46.8	0.7848	44.1	0.4532
0.55	**41.8**	44.8	0.4132	49.2	0.8043	**46.6**	0.6087	48.5	0.7652	45.3	0.4523
0.49	**44.3**	45.7	0.4089	50.4	0.8163	**47.7**	0.6126	49.6	0.7756	46.4	0.4497
0.48	**45.9**	47.4	0.4131	51.7	0.773	**49.4**	0.5931	51.2	0.737	48	0.4491

Transitions (as defined above) from the low field normal state into the field polarized normal state at varying angles from *b* to *c* and base temperature (approximately 500 mK). Data used to construct Fig. 1 in the main text.

Data Processing and Definition of Phase Boundaries – Low-field-superconducting UTe_2

For low-field superconducting crystals, upper critical fields for SC_1 and SC_{FP} were defined from proximity diode oscillator (PDO) measurements as shown in S.7. The metamagnetic transition was defined as the point of maximum slope change, and found by evaluation of the first derivative of the frequency vs applied field curves.

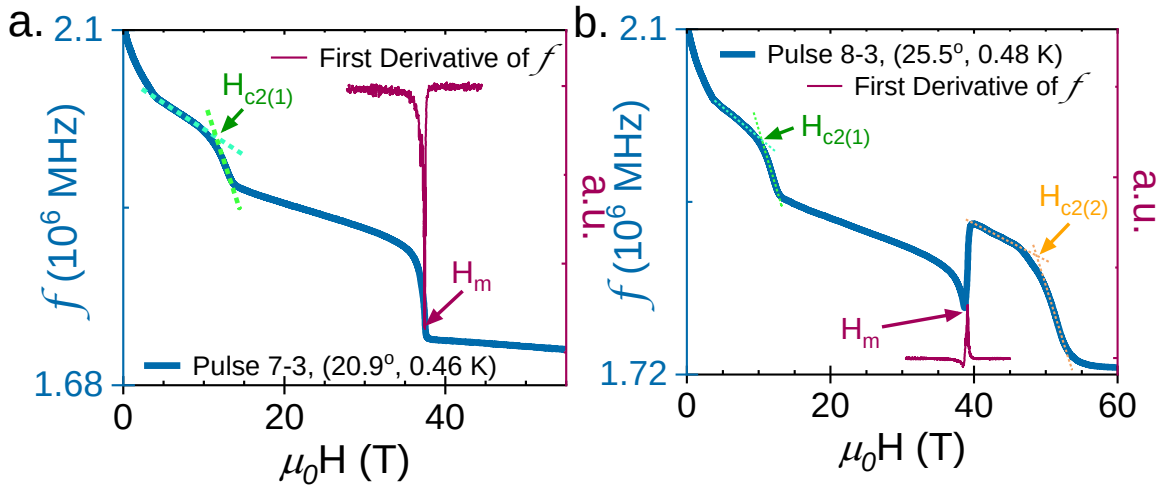

Figure S 7 Example of phase boundary identification showing transitions from SC_1 to the low field normal state and from the low field normal state to (a.) the field polarized normal phase or (b.) SC_{FP} in RRR = 64 samples determined from proximity diode oscillator experiments on field superconducting UTe_2 at base temperature (approximately 500 mK).

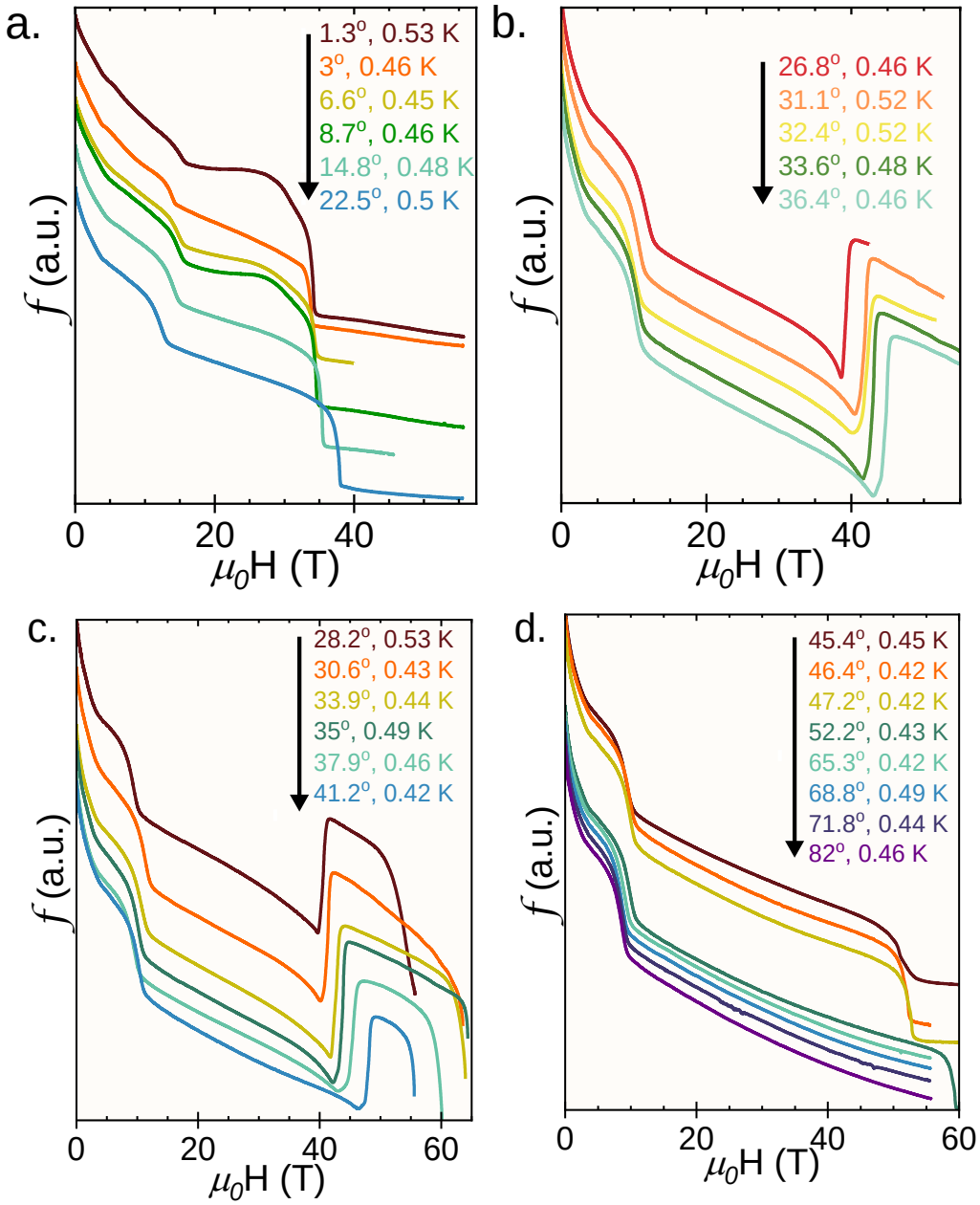

Figure S 8 Base-temperature PDO curves for RRR = 64 low-field-superconducting UTe_2 measured at field orientations offset from crystallographic *b* to *c* by 1.3° – 22.5° (a.), 26.8 ° – 36.4° (b.), 28.2 ° – 41.2° (c.), or 45.4° – 82° (d.). In all cases, vertical units are arbitrary, as individual curves are offset in the in the y axis for visual clarity. Data used to prepare Figure 2 in the main text.

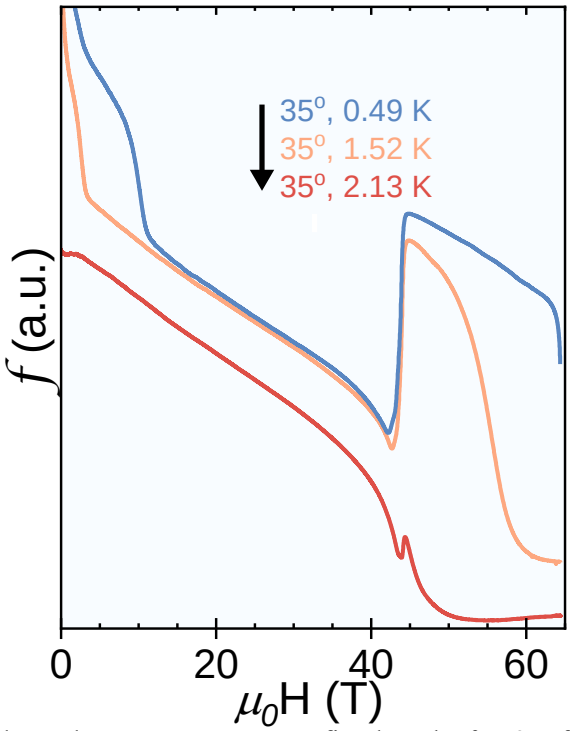

Figure S 9 Temperature dependent PDO curves at a fixed angle, θ = 35° from *b* to *c*, as measured for RRR = 64 low-field-superconducting UTe_2. Vertical units are arbitrary, as individual curves are offset in the in the y axis for visual clarity. Data used to prepare Figure 3 in the main text.

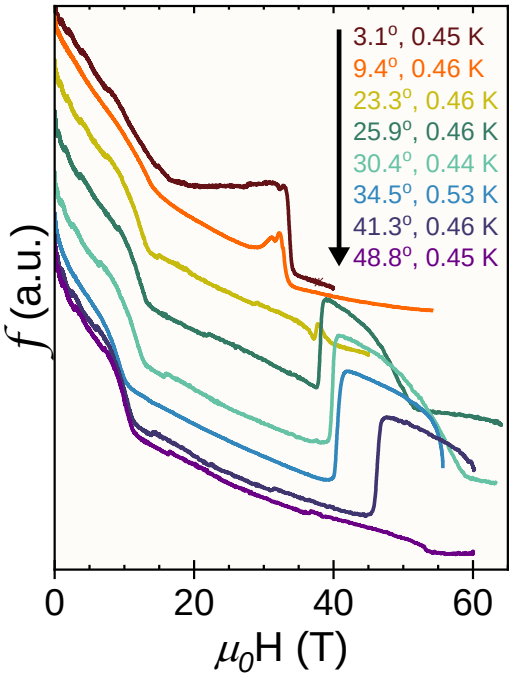

Figure S 10 Angle dependent PDO curves at low temperature as measured for "low" quality (RRR = 8) low-field-superconducting UTe_2. Vertical units are arbitrary, as individual curves are offset in the in the y axis for visual clarity. Data used to prepare Figure 2 in the main text.

Table S. 6 Summary of Phase Transitions from PDO Measurements of RRR = 64 UTe_2

Temp (K)	Angle θ (°)	$H_{c2}(SC_1)$ $\mu_0 H$ (T)	H_m (to FP) $\mu_0 H$ (T)	H_m (to SC_{FP}) $\mu_0 H$ (T)	H_{c2} (SC_{FP}) R (Ω)
0.53	1.3	13.8	34.1		
0.46	3	13.0	33.8		
0.45	6.6	13.6	34.3		
0.46	8.7	13.7	34.6		
0.48	14.8	12.8	35.4		
0.46	20.9	11.3	37.4		
0.5	22.5	10.8	37.9		
0.52	23.9	10.6	37.6		
0.48	25.5	10.3		39.1	48.4
0.46	26.8	10.2		39.3	
0.53	28.2	8.1		40.6	51.8
0.46	29.4	9.5		40.3	53.7
0.43	30.6	10.0		41.3	
0.52	31.3	9.3		42.0	
0.52	32.4	8.6		42.2	
0.48	33.6	9.3		43.1	
0.44	33.9	9.1		42.9	61.3
0.49	34.9	8.9		43.9	64.1
1.52	34.9	2.0		44.0	52.4
2.13	34.9	-		44.5	44.5
0.46	36.4	9.0		44.9	
0.46	37.9	8.1		45.5	58.7
0.42	41.2	8.9		48.1	54.1
0.45	45.4	8.0	50.9		
0.42	46.4	8.7	52.1		
0.42	47.2	8.7	52.7		
0.43	52.2	8.7	59.4		
0.42	65.3	7.7			
0.49	68.8	7.4			
0.44	71.8	7.5			
0.46	82	7.4			

Table S. 7 Summary of Phase Transitions from PDO Measurements of RRR = 8 UTe_2

Temp (K)	**Angle θ (°)**	$H_{c2}(SC_1)$ $\mu_0 H$ (T)	H_m (Normal to FP Normal) $\mu_0 H$ (T)	H_m (Normal to SC_{FP}) $\mu_0 H$ (T)	H_{c2} (SC_{FP}) R (Ω)
0.45	3.1	9.2	33.7	--	--
0.46	9.4	10.2	32.8	--	--
0.46	23.3	10.1		37.5	37.9
0.46	25.9	10.5		38.1	46.2
0.44	30.4	9.5		39.8	51.3
0.53	34.5	7.9		40.4	54.8
0.46	41.3	8.4		46.3	59.4
0.45	48.8	8.7	53.2	--	--